Journal of Electronic Research and Application, 2026, Volume 10, Issue 6
http://ojs.bbwpublisher.com/index.php/JERA
Online ISSN: 2208-3510
Print ISSN: 2208-3502

# A Vessel Segmentation Method Based on Prior-Guided False Positive Suppression Gating

**Jintao Zhang**

College of Computer and Information Engineering, Henan University of Economics and Law, Zhengzhou 450046, Henan, China



**Abstract:** Vessel segmentation is a fundamental task in medical image analysis and plays an important role in computer-aided diagnosis, lesion localization, vascular morphology analysis, and subsequent three-dimensional reconstruction. However, blood vessels usually exhibit elongated shapes, complex branching patterns, significant scale variations, and locally low contrast. Under challenging conditions such as complex backgrounds, noise interference, and blurred boundaries, tiny vessels are prone to missed detection, while background textures and spurious edges are easily misclassified as vessels, resulting in increased false positives. To address these issues, this paper proposes a prior-guided vessel segmentation method with false positive suppression. The proposed method adopts an encoder-decoder architecture as the backbone and introduces a Vessel False Positive Suppression Gate (VFPSGate) into the skip connections during the decoding stage. By integrating vessel region priors and edge priors, the shallow features are recalibrated in a suppression-oriented manner, thereby reducing the interference of background noise and non-vascular high responses on segmentation results. In addition, a Vessel False Positive Suppression Loss (VFPSLoss) is designed to impose extra constraints on abnormally high responses in background regions that are not supported by the priors, thus enhancing the model's targeted suppression ability against false positives at the optimization level. Experimental results on the DCA dataset demonstrate that the proposed method achieves competitive performance, with IoU, DSC, ACC, and SEN reaching 66.49%, 79.72%, 97.88%, and 85.16%, respectively. Overall, the proposed method can more effectively distinguish real vessels from pseudo-vessels, providing a feasible solution for vessel segmentation under complex background conditions.

**Keywords:** Vessel segmentation; Medical image analysis; False positive suppression; Prior guidance

**Online publication:** Jul 23, 2026

## 1. Introduction

Cardiovascular diseases are among the major threats to human health worldwide, and medical image analysis plays an essential role in early disease screening, accurate diagnosis, and treatment evaluation [1–3]. As one of the fundamental tasks in medical image analysis, vessel segmentation has important clinical applications in various scenarios, including retinal imaging, cerebral angiography, pathological sections, and X-ray angiography [4]. On the one hand, accurate vessel extraction can provide clinicians with clear anatomical structural information and support quantitative analysis of morphological indicators such as vessel diameter, curvature, and bifurcation angle, thereby offering reliable evidence for computer-aided diagnosis and lesion localization [5,6]. On the other hand, high-quality two-dimensional vessel segmentation is also a critical prerequisite for subsequent three-dimensional vascular network reconstruction, hemodynamic analysis, and related computer-assisted surgical planning [7,8].

However, vessel structures usually exhibit characteristics such as elongated morphology, complex branching patterns, significant scale variations, and locally low contrast, which make vessel segmentation a challenging task [9,10]. In particular, under conditions of complex backgrounds, imaging noise, and blurred boundaries, tiny vessels are prone to discontinuity or omission, while background textures, noisy edges, and other non-vascular high-response regions are often incorrectly identified as vessels, leading to increased false positives [11,12]. Such false detections not only reduce segmentation accuracy but may also disrupt vascular topological continuity and interfere with subsequent morphological measurement and clinical quantitative analysis [13]. Therefore, how to effectively suppress false positives while preserving real vessel details as much as possible has become a key issue in current vessel segmentation research.

Early vessel segmentation methods mainly relied on handcrafted features, such as region growing, threshold-based segmentation, filtering enhancement, and morphological rules. Although these methods can achieve certain effects in specific scenarios, their generalization ability is usually limited due to their strong dependence on imaging conditions and expert-designed rules [14,15]. With the rapid development of deep learning, especially the wide application of convolutional neural networks based on encoder-decoder architectures in medical image segmentation, the performance of vessel segmentation has been significantly improved [16–18]. In recent years, the introduction of attention mechanisms, Transformers, and related global modeling techniques has further enhanced the representation capability of models for multi-scale features and long-range dependencies, providing new technical pathways for the extraction of complex vascular structures [19,20].

Despite the substantial progress achieved by existing methods in vascular feature representation and structural recovery, explicit modeling of false-positive regions remains relatively insufficient. Specifically, although skip connections in the decoding stage can supplement rich spatial detail information, they may also transmit background textures, noisy edges, and non-vascular high responses into the subsequent segmentation process, thereby increasing the risk of false detections [21]. Meanwhile, most existing methods still rely primarily on data-driven feature learning, and the joint utilization of vessel region priors and boundary priors remains inadequate. As a result, explicit structural constraints for distinguishing real vessel responses from background pseudo-responses are still lacking. In terms of loss function design, commonly used losses such as cross-entropy loss and Dice loss focus more on overall pixel classification accuracy or regional overlap, but lack targeted optimization mechanisms for the specific error type of false positives [22]. In summary, existing methods have paid more attention to enhancing vessel representation, while relatively less effort has been devoted to systematically suppressing false positives from both the perspectives of structural constraints and objective function design.

To address the above issues, this paper proposes a prior-guided false-positive suppression framework for vessel segmentation. In the decoding stage, vessel region priors and edge priors are introduced to construct a

Vessel False Positive Suppression Gate (VFPSGate), which performs suppression-oriented recalibration on shallow features in the skip connections. By leveraging prior information, the proposed module identifies and filters potential false-positive regions, effectively suppressing interference caused by background textures and pseudo-edges while preserving responses that are more likely to correspond to real tiny vessels. Furthermore, a Vessel False Positive Suppression Loss (VFPSLoss) is designed to impose additional constraints on abnormally high responses in background regions that are not supported by the priors, thereby enhancing the model's false-positive suppression capability at the optimization level. Through the collaboration between architectural design and loss design, the proposed method can more effectively distinguish real vessels from pseudo-vessels under complex background conditions, thereby improving the accuracy, completeness, and robustness of vessel segmentation results.

## 2. Method

This section describes in detail the proposed prior-guided false-positive suppression method for vessel segmentation. Overall, the proposed framework suppresses false positives in vessel segmentation through the joint design of network architecture and optimization objective. First, auxiliary information, including a vessel region prior and an edge prior, is constructed to provide explicit region-level and boundary-level structural constraints. Second, VFPSGate is introduced into the skip connections of the encoder-decoder framework to perform suppression-oriented recalibration of shallow features. Finally, VFPSLoss is further designed to enhance the model's targeted suppression ability against background false detections from the perspective of the optimization objective.

### 2.1. Overall framework

As shown **in Figure 1**, the proposed method adopts a classical encoder-decoder architecture as the backbone and further incorporates a prior-guided false-positive suppression mechanism. The encoder progressively extracts multi-scale contextual semantic features through multiple convolutions and downsampling operations, while the decoder gradually restores spatial resolution through layer-by-layer upsampling and feature fusion to generate the final vessel segmentation result. Unlike the conventional U-Net, which directly transmits shallow encoder features to the decoder through skip connections, the proposed method embeds VFPSGate into the skip connections at multiple decoding stages to selectively filter and recalibrate shallow features, thereby reducing the interference of background textures, noisy edges, and non-vascular high-response regions during subsequent decoding.

Specifically, given an input image, the encoder first extracts feature representations at different scales. During decoding, before each decoder feature is fused with its corresponding encoder feature, the encoder feature is first modulated by VFPSGate. At the current scale, this module jointly exploits encoder features, decoder features, and the vessel region prior and edge prior constructed from the input image to perform false-positive suppression-oriented recalibration of shallow features. The gated features are then fused with decoder features for subsequent segmentation recovery. Meanwhile, during training, a dedicated false-positive suppression loss is introduced to cooperate with the structural gating mechanism, so as to further reduce false detections under complex backgrounds while preserving real tiny vessel structures.

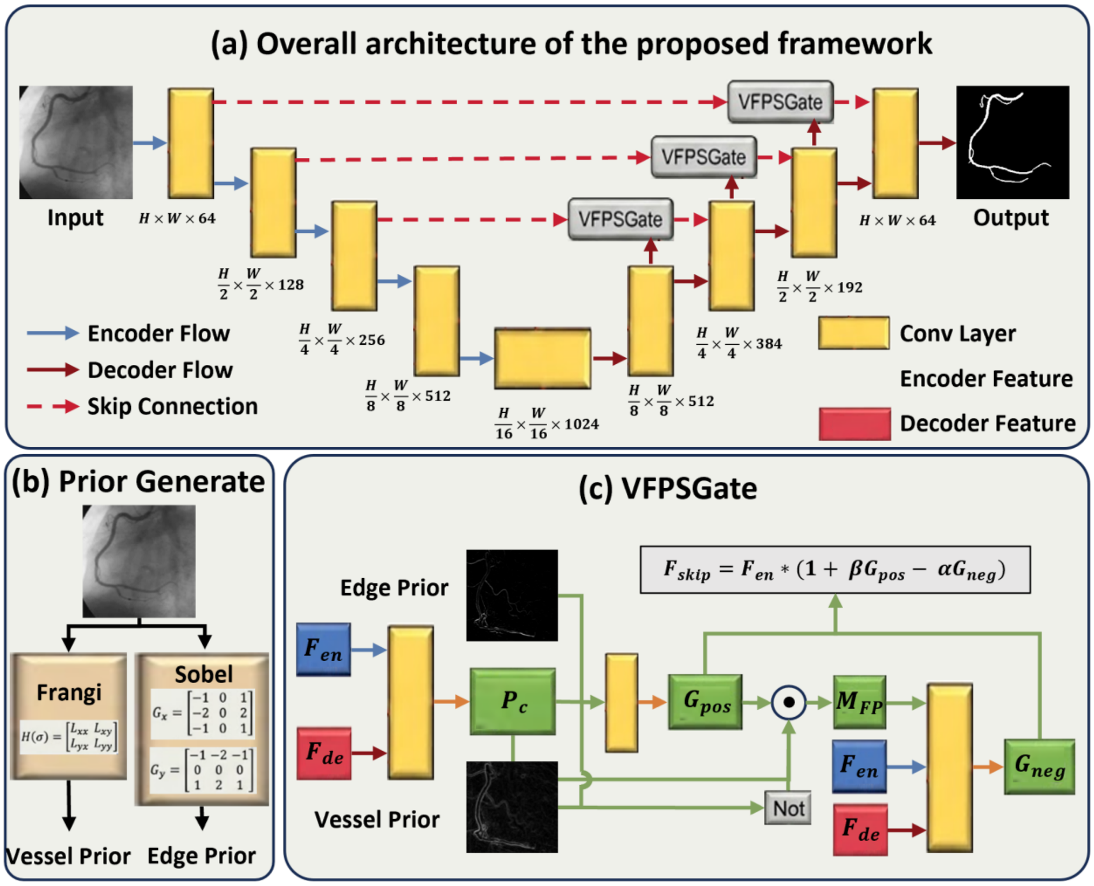


**Figure 1.** Overall framework of the proposed method.

## 2.2. Prior construction

To provide explicit region-level and boundary-level structural constraints for the network, a vessel region prior and an edge prior are constructed based on the input image, as shown in **Figure 1**. Different from purely data-driven feature learning, explicit priors provide more direct structural guidance before the gating process, thereby helping the model better distinguish real vessel responses from background pseudo-responses. Considering that vessels typically exhibit elongated, continuous, and tubular structures, while their boundaries are easily affected by noise and pseudo-edges under complex backgrounds, prior information is constructed from both region enhancement and boundary supplementation perspectives to improve the ability of the subsequent gating module to identify real vascular structures.

For the vessel region prior, since vessels in medical images usually appear as elongated and continuous tubular structures, the Frangi filter is employed to enhance the input image and highlight vessel-like responses [23]. The Frangi filter selectively enhances tubular structures based on the eigenvalues of the Hessian matrix and is able to emphasize regions consistent with vessel morphology under multi-scale settings. Compared with general edge detection or intensity enhancement methods, the Frangi filter focuses more on the geometric characteristics of the target rather than solely on local intensity variations, thereby providing relatively stable candidate information for vessel regions. After normalization, the resulting map is regarded as the vessel region prior. $P_v$, which indicates the prior likelihood of each location belonging to a vessel region.

For the edge prior, to further supplement local variation information related to vessel boundaries, contours, and fine structures, the Sobel operator is used to compute the gradient magnitude of the input image [24]. After normalization, the resulting map is regarded as the edge prior $\mathrm{P}_{\mathrm{e}}$ . The Sobel operator can effectively reflect the intensity of local grayscale changes and is sensitive to fine boundaries and contour transitions, making it suitable as boundary-level structural supplementary information. Different from the vessel region prior, which mainly provides regional support, the edge prior pays more attention to local boundary variation and structural continuity, and can provide additional contour discrimination cues in regions with low contrast, blurred boundaries, or complex background textures.

Overall, the vessel region prior and the edge prior are highly complementary. The former emphasizes regional consistency and the distribution of tubular structures, whereas the latter emphasizes boundary rationality and local contour continuity. By jointly introducing these two types of priors, the model can not only determine whether a location is likely to belong to a vessel region, but also further assess whether it exhibits a plausible boundary pattern. These two priors are finally fed into the subsequent VFPSGate to provide explicit guidance for positive gating construction and false-positive suppression from both region and boundary perspectives, thereby enhancing the model's ability to distinguish real vessels from pseudo-vessels under complex background conditions.

## 2.3. Vessel false positive suppression gate

In a standard encoder-decoder architecture, skip connections provide rich, shallow detail information for the decoder, which is crucial for recovering tiny vessels. However, while preserving textures and edge information, shallow features may also contain background noise, pseudo-edges, and other non-vascular high-response regions. If such features are directly passed to the decoder, they may amplify false positives during subsequent segmentation. To address this issue, the proposed VFPSGate performs prior-guided recalibration of shallow encoder features in the skip connections. By combining decoder features, the vessel region prior, and the edge prior, the module identifies and suppresses potential false-positive regions while retaining responses that are more likely to correspond to real vessels. The overall computational process is illustrated in **Figure 1**.

First, at the current scale, the encoder feature $F_{en}$ and the decoder feature $F_{de}$ are fused, and a coarse vessel prediction is generated through a lightweight prediction branch $P_c$ :

$$P_c = \sigma\left(f_c\left(\left[F_{en}, F_{de}\right]\right)\right) \tag{1}$$

where $[\cdot]$ denotes channel-wise concatenation, $f_c(\cdot)$ denotes the coarse vessel prediction branch, and $\sigma(\cdot)$ denotes the Sigmoid activation function. $P_c$ is not the final segmentation output, but rather an initial estimation of vessel regions at the current scale, which serves as the basis for subsequent false-positive candidate localization.

After obtaining the coarse vessel probability map, the vessel region prior $P_v$ and the edge prior $P_e$ are further incorporated to construct a positive gating branch, which is used to select responses that are more likely to correspond to real vessels from the perspectives of both regional consistency and boundary structural rationality. The positive gate $G_{pos}$ is generated jointly from the coarse vessel prediction and the two priors:

$$G_{pos} = \sigma\left(f_p\left(\left[P_c, P_v, P_{\mathrm{e}}\right]\right)\right) \tag{2}$$

where $f_p(\cdot)$ denotes the positive gate generation branch. Different from relying solely on the coarse prediction, the positive gate simultaneously integrates region-level and boundary-level prior constraints, thereby more effectively highlighting responses associated with real vessels and providing guidance for the construction of subsequent false-positive candidate regions.

Based on the principle that the model may produce high responses in regions unsupported by the priors, a false-positive candidate map $M_{FP}$ is further constructed. If a location exhibits a high response in the coarse vessel prediction and still maintains strong vessel-related activation after positive gating, but shows a weak response in the vessel region prior, then this location is more likely to correspond to a false-positive background response rather than a real vessel. The false-positive candidate map $M_{FP}$ is defined as

$$M_{FP} = G_{pos} \odot P_{c} \odot \left(1 - P_{v}\right) \tag{3}$$

where $\odot$ denotes element-wise multiplication. This design explicitly extracts suspicious regions that the model considers vessel-like but are not supported by the vessel prior, thereby providing direct evidence for the subsequent negative suppression gate.

Subsequently, a negative gating branch is constructed using. $F_{en}$, $F_{de}$, and $M_{FP}$ to suppress responses that are more likely to be background false detections. The negative gate is formulated as

$$G_{neg} = \sigma\left(f_n\left(\left[F_{en}, F_{de}, M_{FP}\right]\right)\right) \tag{4}$$

where $f_n(\cdot)$ denotes the negative gate generation branch. Unlike the positive gate, which focuses on preserving real vessel responses, the negative gate is specifically designed to model potential false-positive regions, thereby enabling explicit suppression of background high responses and pseudo-edge interference.

Finally, to preserve real vessel details while suppressing false-positive background responses, an asymmetric recalibration strategy is adopted to update the shallow encoder features:

$$F_{skip} = F_{en} \odot \left(1 + \beta G_{pos} - a G_{neg}\right) \tag{5}$$

where $F_{skip}$ denotes the gated skip connection feature, $\alpha$ and $\beta$ are learnable parameters. According to preliminary experiments, they are initialized as 2.0 and -1.0, respectively. Through this asymmetric dual-path gating mechanism, VFPSGate can preserve fine vessel and boundary details while effectively reducing the interference of background textures, noisy edges, and non-vascular high-response regions during subsequent decoding, thereby improving the accuracy and structural integrity of vessel segmentation under complex backgrounds.

## 2.4. Vessel false positive suppression loss

To further enhance the model's targeted suppression ability against false-positive regions, a Vessel False Positive Suppression Loss is designed and jointly optimized with VFPSGate. Different from traditional segmentation losses that rely only on final output supervision, the overall loss function in this work simultaneously considers the final segmentation output, intermediate coarse vessel predictions, and background false-detection penalties, thereby constraining the learning process from both output-level and intermediate-level perspectives.

First, the main segmentation loss is used to constrain the consistency between the final output and the ground-truth label. In this work, a combination of binary cross-entropy (BCE) loss and Dice loss is adopted as the basic supervision term to account for pixel-level classification accuracy and region overlap quality jointly [25,26]

$$L_{main} = L_{BCE}\left(\hat{Y}, \mathrm{Y}\right) + L_{Dice}\left(Y, \mathrm{Y}\right) \tag{6}$$

where $\hat{Y}$ denotes the final prediction and Y denotes the ground-truth label.

Second, to improve the reliability of the intermediate coarse vessel predictions in each VFPSGate, auxiliary supervision is imposed on the coarse predictions at multiple decoding stages. Let $P_c^{(k)}$ denote the coarse vessel prediction at the k-th scale and $Y_c^{(k)}$ denote the corresponding ground-truth label at that scale. The auxiliary supervision loss is defined as

$$L_{aux} = \frac{1}{K}\sum_{k=1}^{K} L_{seg}(P_{\chi}^{(\kappa)}, Y_{\chi}^{(\kappa)}) \tag{7}$$

where K denotes the number of VFPSGate modules involved in auxiliary supervision. Consistent with the main segmentation loss, the auxiliary loss also adopts the combination of BCE loss and Dice loss. By applying segmentation supervision to these intermediate predictions, they are not merely internal variables of the gating module, but also carry explicit vessel semantic information. More reliable coarse predictions contribute to more stable positive gating construction and false-positive candidate generation, thereby enhancing the stability and interpretability of the entire gating mechanism.

On this basis, a false-positive penalty term is further designed to constrain regions that satisfy the following conditions explicitly: they belong to the background in the ground-truth label, are not supported by the vessel region prior, but still receive high responses in the coarse vessel prediction. For the k-th scale, if a location corresponds to the background in $Y^{(k)}$ It has a low response in $P_v^{(k)}$, but still exhibits a high value in $P_c^{(k)}$ Then the model tends to misclassify this background region as a vessel. Accordingly, the multi-scale false-positive penalty term is defined as

$$L_{fp} = \frac{1}{K}\sum_{k=1}^{K} \frac{\sum(1\text{-}Y^{(k)})(1\text{-}P_v^{(k)})P_c^{(k)}}{\sum(1 - Y^{(k)}) + \epsilon} \tag{8}$$

where K is the number of scales involved in auxiliary supervision, $Y^{(k)}$, $P_v^{(k)}$, $P_c^{(k)}$ and denote the ground-truth label, vessel region prior, and coarse vessel prediction at the k-th scale, respectively, and $\epsilon$ is a smoothing constant. This loss term imposes an additional penalty on locations in background regions that violate prior constraints, thereby enabling targeted suppression of false positives. Unlike traditional segmentation losses, which mainly focus on overall region overlap, this term directly addresses the specific error type of "background being misclassified as vessel," and is therefore more consistent with the design objective of this work.

Finally, the main segmentation loss, auxiliary supervision loss, and false-positive penalty term are combined in a weighted manner to form the overall optimization objective:

$$L = L_{main} + \lambda_{aux} L_{aux} + \lambda_{fp} L_{fp} \tag{9}$$

where $\lambda_{aux}$ and $\lambda_{fp}$ denote the weighting coefficients for the auxiliary supervision term and the false-positive penalty term, respectively. Through the joint optimization of these loss terms, the network is able not only to learn more accurate vessel segmentation representations but also to explicitly reduce abnormally high responses in prior-unsupported regions during training, thereby improving the accuracy, completeness, and robustness of vessel segmentation results under complex background conditions.

# 3. Results

## 3.1. Experimental settings and evaluation metrics

Experiments were conducted on the DCA dataset to validate the effectiveness of the proposed method [27]. This dataset contains coronary angiography images and their corresponding vessel segmentation annotations, and can well reflect practical segmentation challenges such as complex backgrounds, low contrast, and abundant fine vessel structures. The dataset was divided into training, validation, and test sets with a ratio of 7:1:2. To improve the generalization ability of the model, data augmentation strategies including random 90°

rotation, random horizontal flipping, and random vertical flipping were adopted during training. All input images were resized to 256 × 256.

To comprehensively evaluate the effectiveness of the proposed method, several representative medical image segmentation models were selected for comparison, including the classical convolutional architectures UNet, ResUNet, UNet++, the attention-based Attention UNet, and models with stronger feature modeling capability, including TransUNet, Swin UMamba, and UKAN [28–34]. For fair comparison, all methods were trained and tested under the same dataset and unified experimental settings.

To assess segmentation performance from different perspectives, Intersection over Union (IoU), Dice Similarity Coefficient (DSC), Accuracy (ACC), and Sensitivity (SEN) were adopted as evaluation metrics [35–38]. Among them, IoU and DSC mainly reflect the overlap between the prediction and the ground truth, ACC measures overall pixel-wise classification accuracy, and SEN emphasizes the detection ability for true vessel regions, thereby better reflecting the model's capability to preserve fine vessels and low-contrast vessels.

All experiments were implemented in PyTorch and conducted on an NVIDIA RTX 4090 GPU. During training, the batch size was set to 8, and the initial learning rate was set to $1\times10^{-4}$ The Adam optimizer was adopted, and the total number of training epochs was 400. For loss function configuration, VFPSLoss was used as the overall optimization objective, where the weight of the auxiliary supervision term $\lambda_{aux}=0.2$, and the weight of the false-positive penalty term $\lambda_{fp}=0.05$.

## 3.2. Comparison experiments

**Table 1** presents the quantitative comparison results between the proposed method and several mainstream segmentation models on the DCA dataset. As can be seen, the proposed method achieved the best performance across all evaluation metrics. Specifically, the proposed method reached 66.49%, 79.72%, 97.88%, and 85.16% in terms of IoU, DSC, ACC, and SEN, respectively. These results indicate that the proposed method not only improves the overall overlap quality of segmentation but also enhances the detection ability for vessel regions.

**Table 1.** Quantitative comparison of different methods for vessel segmentation on the DCA dataset

| | IOU | DSC | ACC | SEN |
|---|---|---|---|---|
| UNet | 65.43 | 78.95 | 97.85 | 82.53 |
| ResUNet | 65.59 | 79.08 | 97.84 | 83.48 |
| UNet++ | 65.99 | 79.33 | 97.85 | 84.26 |
| Attention UNet | 66.22 | 79.54 | 97.85 | 84.89 |
| TransUNet | 66.39 | 79.67 | 97.90 | 84.19 |
| Swin UMamba | 63.90 | 77.83 | 97.68 | 83.84 |
| UKAN | 65.34 | 77.58 | 97.68 | 81.76 |
| Our | 66.49 | 79.72 | 97.88 | 85.16 |

From the performance trends, the improvements achieved by the proposed method are particularly noticeable in terms of DSC and SEN. The improvement in DSC indicates a higher overall overlap between the prediction and the ground-truth vessel region, while the clear gain in SEN suggests that the proposed method is more effective in preserving real vessels, especially fine vessels, low-contrast vessels, and branching structures. Considering that there is usually a trade-off between fine-detail recovery and false-positive suppression in vessel segmentation, the proposed method still maintains relatively high ACC and IoU while improving SEN. This indicates that the gain in sensitivity is not achieved by simply enlarging the predicted vessel regions, but rather by effectively suppressing false-positive responses in background regions while preserving real vessels.

These results are consistent with the design objective of the proposed method. First, the vessel region prior provides region-level structural support, helping the model emphasize candidate regions that are more consistent with tubular morphology. Second, the edge prior further supplements local contour and boundary information, enabling the model to distinguish real vessel boundaries from background pseudo-edges better. Finally, VFPSLoss imposes additional penalties on regions that belong to the background and are unsupported by the prior but still receive high model responses, thereby further reducing false detections at the optimization level. As a result, the structural gating mechanism and the targeted loss constraint complement each other, endowing the model with a stronger capability to identify real vessels and suppress false positives under complex background conditions.

To provide a more intuitive comparison of segmentation performance, **Figure 2** shows the visualization results of different methods on two representative samples. As can be observed, although the compared methods can extract the main vessel trunks to a certain extent, they still show deficiencies in recovering fine branches, curved boundaries, and low-contrast regions, and may also produce false detections in local background areas. In contrast, the proposed method achieves better performance in terms of main trunk continuity, fine branch completeness, and background suppression.

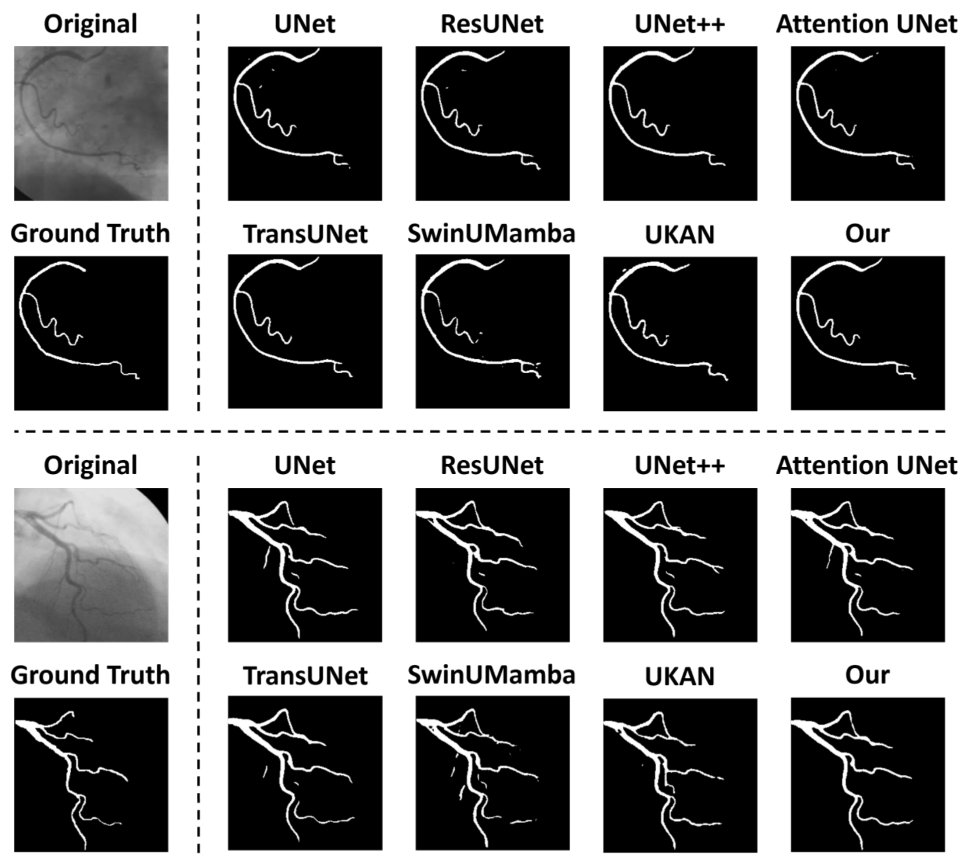


**Figure 2.** Visual comparison of vessel segmentation results produced by different methods.

Specifically, in the first sample, the proposed method preserves the fine branches within the curved main trunk more completely, produces smoother and more continuous segmentation contours, and yields fewer scattered false responses in the background. In the second sample, when faced with regions containing more bifurcations and more complex structures, the proposed method better maintains the connectivity among branches while reducing erroneous responses in non-vascular regions. Overall, the segmentation results generated by the proposed method are cleaner, more continuous, and more consistent with the true morphological characteristics of vessels.

### 3.3. Ablation studies

To further verify the individual contributions of each component and their collaborative effect, ablation studies were conducted on the DCA dataset. Specifically, based on the baseline model, the vessel region prior, the edge prior, the false-positive suppression loss, and the complete model were introduced step by step. The experimental results are shown in **Table 2**.

**Table 2.** Ablation study of different components of the proposed method on the DCA dataset

| Vessel | Edge | VFPSLoss | IOU | DSC | ACC | SEN |
|---|---|---|---|---|---|---|
| - | - | - | 65.43 | 78.95 | 97.85 | 82.53 |
| √ | | | 66.31 | 79.57 | 97.92 | 82.63 |
| √ | √ | | 66.03 | 79.38 | 97.90 | 82.71 |
| √ | | √ | 66.09 | 79.43 | 97.84 | 85.06 |
| √ | √ | √ | 66.49 | 79.72 | 97.88 | 85.16 |

Each component improves the model performance to a certain extent. When only the vessel region prior is introduced, IoU, DSC, and ACC all improve, indicating that the region prior can provide effective structural guidance for the model. After introducing the false-positive suppression loss, SEN increases from 82.53% to 85.06%, demonstrating that this loss plays an important role in both real vessel detection and background false-positive suppression. In comparison, the improvement brought by the edge prior alone is relatively limited, but it still provides useful supplementary information for local contour and boundary modeling.

When the vessel region, edge prior, and false-positive suppression loss are used together, the complete model achieves the best performance. Compared with the baseline, IoU, DSC, ACC, and SEN are improved by 1.05%, 0.77%, 0.03%, and 2.63%, respectively. These results indicate that the proposed components are complementary to each other and can collaboratively suppress false positives from both the perspectives of structural constraint and optimization objective, thereby improving the overall vessel segmentation performance.

## 4. Discussion

The experimental results on the DCA dataset demonstrate that the proposed prior-guided false-positive suppression strategy can effectively improve vessel segmentation performance. By combining quantitative results with visual analysis, it can be observed that the proposed method not only improves the overlap between the predictions and the ground truth but also enhances the detection of fine vessels, low-contrast vessels, and complex branching structures. Meanwhile, the visualization results further show that, while maintaining the continuity of the main vessel trunks and the integrity of fine branches, the proposed method can more effectively reduce scattered false responses and erroneous connections in background regions. These findings indicate that the performance gain of the proposed method does not stem from simply enlarging the predicted vessel area, but rather from the simultaneous enhancement of real vessel preservation and background false-positive suppression.

From the perspective of the method design, this performance improvement mainly benefits from the collaboration between the architectural design and the loss design. On the one hand, the vessel region provides region-level structural support, enabling the network to focus more on candidate regions that are consistent with tubular morphology. The edge prior further supplements local contour and boundary information, thereby improving the discrimination between real vessel boundaries and background pseudo-edges. On the other hand, VFPSGate performs suppression-oriented recalibration of shallow features in the skip connections, which helps preserve fine details while weakening the interference caused by noisy textures and non-vascular high responses. In addition, VFPSLoss imposes additional constraints on high responses in background regions that are not supported by the priors, thereby enhancing the model's targeted suppression ability against false-positive regions at the optimization level. The fact that the complete model achieves the best performance in the ablation experiments also indirectly verifies the good complementarity among the proposed components.

Another advantage of the proposed method lies in its practicality and scalability. For tasks such as coronary angiography, where the background is complex, the boundaries are ambiguous, and fine vessels are abundant, reducing false positives is beneficial not only for improving segmentation accuracy but also for enhancing the reliability of subsequent morphological analyses such as vessel diameter, curvature, and bifurcation measurement. Moreover, the prior-guided false-positive suppression idea proposed in this work does not rely on a specific backbone network. In principle, it can be conveniently transferred to other encoder-decoder-based segmentation frameworks, indicating a certain degree of general applicability.

Nevertheless, the proposed method still has some limitations. First, the model performance depends to some extent on the quality of the vessel region prior to and the edge prior to. When the input image contains stronger noise or even lower contrast, the priors themselves may be degraded, which may further weaken the gating effect. Second, in regions containing extremely weak vessels, severe structural overlap, or complex lesion interference, the difference between real vessel responses and background pseudo-responses may still be subtle, leaving room for further improvement in discrimination capability. Finally, the experiments in this work were mainly conducted on the DCA dataset, and the cross-dataset generalization ability of the proposed method has not yet been systematically evaluated on more diverse vessel segmentation tasks.

Future work can be carried out in three directions. First, more adaptive prior construction strategies can be explored, extending the current priors generated by traditional image processing methods to learnable or dynamically updated prior representations. Second, based on false-positive suppression, topological continuity or structural consistency constraints can be further introduced to better balance fine vessel preservation and overall connectivity. Third, the proposed framework can be extended to retinal vessel, cerebrovascular, and other multimodal vessel segmentation tasks to validate its generality and clinical application potential further.

## 5. Conclusion

This paper proposes a prior-guided false-positive suppression framework to address the problems of missed detection of fine vessels and increased false positives under complex backgrounds in vessel segmentation. The proposed method introduces VFPSGate into the skip connections of the encoder-decoder architecture and combines vessel region priors and edge priors to recalibrate shallow features. In addition, VFPSLoss is designed to impose extra constraints on abnormally high responses in background regions that are not supported by the priors, thereby effectively reducing background false detections while preserving real vessel details.

Experimental results on the DCA dataset demonstrate that the proposed method achieves competitive performance across multiple evaluation metrics. Quantitative comparisons, visual analyses, and ablation studies further verify the effectiveness of each component and its collaborative effect. Overall, the proposed method can more effectively distinguish real vessels from pseudo-vessels, thereby improving the accuracy and robustness of vessel segmentation under complex background conditions.

## Disclosure statement

The author declares no conflict of interest.

## References


[1] Naser M, Majeed A, Alsabah M, et al., 2024, A Review of Machine Learning's Role in Cardiovascular Disease Prediction: Recent Advances and Future Challenges. Algorithms, 17(2): 78.

[2] Restrepo Tique M, Araque O, Sanchez-Echeverri L, 2024, Technological Advances in the Diagnosis of Cardiovascular Disease: A Public Health Strategy. International Journal of Environmental Research and Public Health, 21(8): 1083.

[3] Sanyaolu S, 2025, Integration of Machine Learning in Imaging Analysis for Clinical Diagnosis of Cardiovascular Diseases. Premier Journal of Cardiology, 2: 100006.

[4] Xia W, et al., 2025, vesselFM: A Foundation Model for Universal 3D Blood Vessel Segmentation. arXiv preprint arXiv:2411.17386.

[5] Oliveira A, Pereira S, 2021, Retinal Vessel Segmentation for Morphological Analysis and Computer-Aided Diagnosis of Cardiovascular Diseases. Medical Image Analysis, 71: 102066.

[6] Khan M, Ahmad B, Soomro S, 2022, Coronary Artery Segmentation and Morphological Quantification for Atherosclerotic Lesion Detection. IEEE Journal of Biomedical and Health Informatics, 26(7): 3104–3114.

[7] Kryvoshei O, Kamencay P, Polak L, 2026, Neural Vessel Segmentation and Gaussian Splatting for 3D Reconstruction of Cerebral Angiography. AI, 7: 22.

[8] Narra S, et al., 2025, A Multi-Stage Deep Learning Pipeline for 3D Coronary Artery Reconstruction from X-Ray Angiograms. IEEE Xplore (Conference Proceedings).

[9] Yuan Y, Zhang Y, Zhu L, et al., 2024, Exploiting Cross-Scale Attention Transformer and Progressive Edge Refinement for Retinal Vessel Segmentation. Mathematics, 12: 264.

[10] Xu B, Yang J, Hong P, et al., 2024, Coronary Artery Segmentation in CCTA Images Based on Multi-Scale Feature Learning. Journal of X-Ray Science and Technology, 32(4): 973–991.

[11] Song R, Liu L, Zhang Y, et al., 2026, VFGS-Net: Frequency-Guided State-Space Learning for Topology-

Preserving Retinal Vessel Segmentation. arXiv preprint arXiv:2602.10978.

[12] Xu H, Meng P, Wang M, et al., 2025, DB-KAUNet: An Adaptive Dual Branch Kolmogorov-Arnold UNet for Retinal Vessel Segmentation. arXiv preprint arXiv:2512.01657.

[13] Wang W, Xia Q, Yan Z, et al., 2024, AVDNet: Joint Coronary Artery and Vein Segmentation with Topological Consistency. Medical Image Analysis, 91: 102999.

[14] Paulauskaite Taraseviciene A, Siaulys J, Jankauskas A, et al., 2025, A Robust Blood Vessel Segmentation Technique for Angiographic Images Employing Multi Scale Filtering Approach. Journal of Clinical Medicine, 14(2): 354.

[15] Zhong Y, Chen T, Zhong D, et al., 2024, Vessel Segmentation in Fundus Images with Multi-Scale Feature Extraction and Disentangled Representation. Applied Sciences, 14(12): 5039.

[16] Kande G, et al., 2024, MSR U-Net: An Improved U-Net Model for Retinal Blood Vessel Segmentation. IEEE Access, 12: 534–551.

[17] Ramos-Cortez J, Alvarado-Carrillo D, Ovalle-Magallanes E, et al., 2025, Lightweight U-Net for Blood Vessels Segmentation in X-Ray Coronary Angiography. Journal of Imaging, 11: 106.

[18] Hernandez-Gutierrez F, Avina-Bravo E, Ibarra-Manzano M, et al., 2025, Retinal Vessel Segmentation Based on a Lightweight U-Net and Reverse Attention. Mathematics, 13: 2203.

[19] Soni T, Gupta S, Bharany S, et al., 2025, Retinal Vessel Segmentation Using Multi-Scale Feature Attention with MobileNetV2 Encoder. Scientific Reports, 15(1): 43369.

[20] Zhang Y, Chung A, 2024, Retinal Vessel Segmentation by a Transformer-U-Net Hybrid Model with Dual-Path Decoder. IEEE Journal of Biomedical and Health Informatics, 28(9): 5347–5359.

[21] Chen S, Fan J, Ding Y, et al., 2024, PEA-Net: A Progressive Edge Information Aggregation Network for Vessel Segmentation. Computers in Biology and Medicine, 169: 107766.

[22] Li A, Sun M, Wang Z, 2024, TD Swin-UNet: Texture-Driven Swin-UNet with Enhanced Boundary-Wise Perception for Retinal Vessel Segmentation. Bioengineering, 11: 488.

[23] Shi G, Lu H, Hui H, et al., 2025, Benefit from Public Unlabeled Data: A Frangi Filter-Based Pretraining Network for 3D Cerebrovascular Segmentation. Medical Image Analysis, 101: 103442.

[24] Bai H, Ma Z, Gao C, et al., 2025, SVSNet: Scleral Vessel Segmentation with a CNN-Transformer Hybrid Network. Journal of Innovative Optical Health Sciences, 18(6): 2550017.

[25] Yeung M, Sala E, Schönlieb C, et al., 2022, Unified Focal Loss: Generalizing Dice and Cross Entropy-Based Losses to Handle Class Imbalanced Medical Image Segmentation. Computerized Medical Imaging and Graphics, 95: 102026.

[26] Yeung M, Rundo L, Nan Y, et al., 2023, Calibrating the Dice Loss to Handle Neural Network Overconfidence for Biomedical Image Segmentation. Journal of Digital Imaging, 36(2): 739–752.

[27] Cervantes-Sanchez F, Cruz-Aceves I, Hernandez-Aguirre A, et al., 2019, Automatic Segmentation of Coronary Arteries in X-Ray Angiograms Using Multiscale Analysis and Artificial Neural Networks. Applied Sciences, 9: 5507.

[28] Shariaty F, Mohebi M, Barzegar-Golmoghani E, et al., 2025, Deep Vessel Segmentation with U-Net and Texture Representation of Image (TRI) Features Provides a Foundation for Improved Objective and Automated Analysis of Coronary Artery Disease from Angiography. Computer Methods and Programs in Biomedicine, 272: 109072.

[29] Amine J, Mourad M, 2025, Toward Accurate Alzheimer's Detection: Transfer Learning with ResNet50 for MRI-Based Diagnosis. Frontiers in Neuroscience, 19: 1664418–1664418.

[30] Zhou Z, Siddiquee M, Tajbakhsh N, et al., 2020, UNet++: Redesigning Skip Connections to Exploit Multiscale Features in Image Segmentation. IEEE Transactions on Medical Imaging, 39(6): 1856–1867.

[31] Cao J, Chen J, Gu Y, et al., 2023, MFA-UNet: A Vessel Segmentation Method Based on Multi-Scale Feature Fusion and Attention Module. Frontiers in Neuroscience, 17: 1249331.

[32] Zhang Y, Chung A, 2024, Retinal Vessel Segmentation by a Transformer-U-Net Hybrid Model with Dual-Path Decoder. IEEE Journal of Biomedical and Health Informatics, 28(9): 5347–5359.

[33] Liu J, et al., 2025, Swin-UMamba: Adapting Mamba-Based Vision Foundation Models for Medical Image Segmentation. IEEE Transactions on Medical Imaging, 44(10): 3898–3908.

[34] Li C, Liu X, Li W, et al., 2025, U-KAN Makes Strong Backbone for Medical Image Segmentation and Generation. Proceedings of the AAAI Conference on Artificial Intelligence, 39(5): 4652–4660.

[35] Prokop K, Polap D, 2024, Image Segmentation Enhanced by Heuristic Assistance for Retinal Vessels Case. Proceedings of IEEE Congress on Evolutionary Computation, Yokohama, Japan: 1–6.

[36] Seker M, Kartal M, Moniri A, et al., 2025, Hepatic Vessel Segmentation and Classification in CTA Images Using nnU-Net with Centerline Regression. Proceedings of IEEE International Workshop on Machine Learning for Signal Processing, Istanbul, Turkiye: 1–4.

[37] Attah M, Elloumi Y, Kachouri R, 2024, High Performance and Low Complexity Retinal Vessel Segmentation Method Based on Extended DCNN. Proceedings of IEEE International Conference on Image Processing Theory, Tools and Applications, Rabat, Morocco: 01–06.

[38] Xu J, Liu Q, Shen J, et al., 2025, Image-Text Guided Fundus Vessel Segmentation via Attention Mechanism and Gated Residual Learning. Frontiers in Cell and Developmental Biology, 13: 1710343.